Statfjord study demonstrates use of neural network to predict porosity and water saturation from time-lapse seismic

Tanja Oldenziel*, Paul de Groot (dGB Earth Sciences) and Leif B. Kvamme (Statoil)

Introduction

With an estimated STOIIP of more than 1 billion m^3, Statfjord is the largest oil discovery in the North Sea to date. Structurally the field is a tilted fault block with Jurassic beds dipping westward at 6 to 8° and truncated on the faulted and eroded East flank (Kirk, 1980 and Fig. 1). The field is divided into three main reservoir units, which are in order of decreasing importance: Brent, Statfjord and Dunlin. Since its discovery in 1974 almost 200 wells have been drilled. The cumulative production from the start of production in 1979 until the end of 1997 was 550 million m^3. This represents approx. 55% of the initial oil in place and 83% of the official recoverable reserves of 662 million m^3. All reservoirs have been partly drained so far during the field's history. In the early years, produced gas was re-injected into the Statfjord reservoir at an up dip position, while the Brent reservoir was depleted until pressure maintenance by down flank water injection was established in 1986. This resulted in extensive gas and water breakthroughs in the production lines and a change in drainage strategy. In the last decade the strategy has been based on in-fill drilling to produce by-passed oil and remaining oil in structural traps and recently in combination with gas and water injection to mobilize remaining oil.

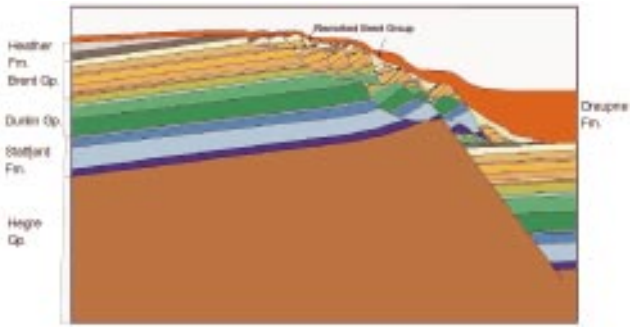

Figure 1 East–West cross-section through the Statfjord field.

To find unswept or by-passed oil three consecutive 3D seismic surveys, acquired in 1979, 1991 and 1997 respectively, have been the basis for seismic monitoring analysis. In this case study, only the latter two surveys were used. The aim of the study was to predict porosity and water saturation at the respective acquisition dates.

For each survey five seismic volumes were available: mid- and far-angle reflectivity, mid- and far-angle elastic impedance, and acoustic impedance. The partial stacked cubes have similar fold and contain angles around 15 and 25°, respectively. The inversion method used was a global search through a simulated annealing scheme using a constant wavelet. Some 130 wells were used, each with an extensive suite of measured logs and 1991 and 1997 time-equivalent logs. The reservoir simulator and a modified Gassmann fluid replacement algorithm were used to compute the time-equivalent logs. For most wells a neural network predicted a measured shear sonic log from measured sonic, density and gamma ray logs.

Volume transformation

Volume transformation is defined as the process of mapping one or more seismic input volumes to one or more output volumes (de Groot, 1999). In this case the information from 10 input volumes was mapped to three output volumes covering the Brent interval. A supervised neural network does the non-linear mapping. The output volumes are porosity and water saturation in 1991 and 1997, respectively. Figure 2 illustrates the process. The input to the neural network is shown schematically. At each sample position the complete waveform rather than some derived attributes was taken from the seismic reflectivity cubes. At the same position the amplitude was extracted from each of the impedance cubes. The network processed this information and predicted the target value(s) for which it was trained. Next it slid one sample position down the various input cubes, extracted the information it needed and predicted the next value(s). And so on, for all samples and all traces in the target zone.

In this case study fully connected Multi-Layer-Perceptron (MLP)-type neural networks were used. The

* Correspondence: dGB Earth Sciences, Boulevard 1945-24, 7511 AE Enschede, the Netherlands; E-mail: tanja@dgb.nl

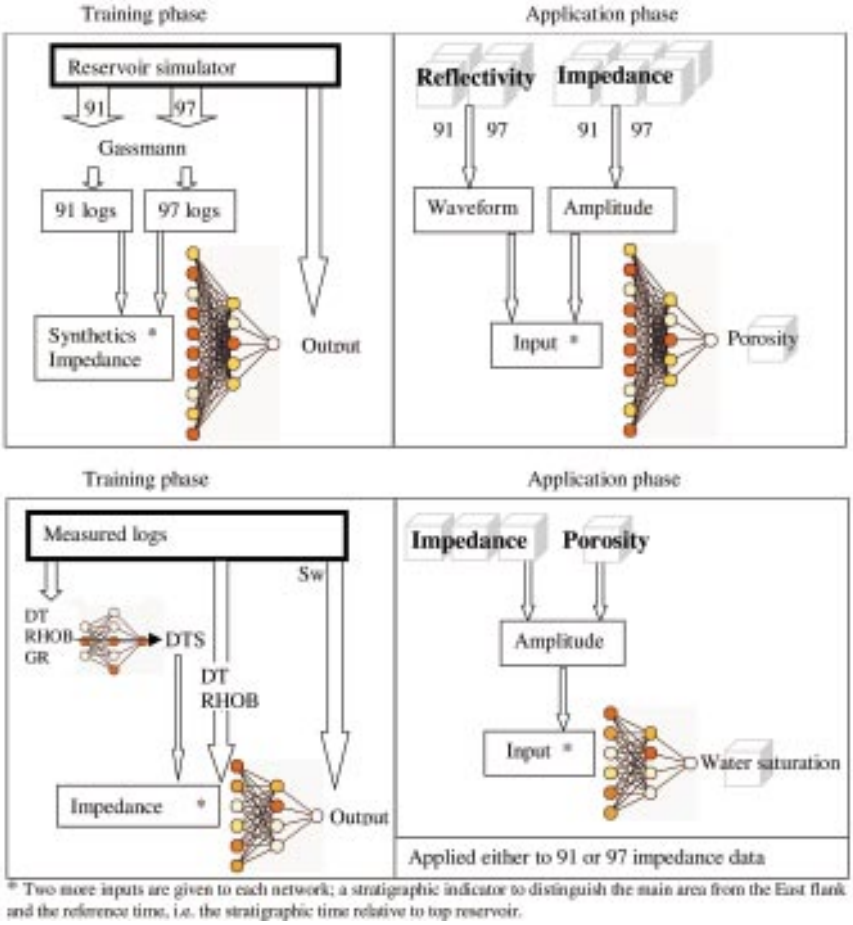

Figure 2 Flow diagram porosity prediction (top) and water saturation prediction (bottom). Impedance means acoustic impedance, and mid and far angle elastic impedance.

networks were trained and tested on examples taken from the real well database in a sliding fashion as described above. The target porosity and water saturation traces were constructed from logs. The relevant logs were converted from depth-to-time using the sonic log and then resampled with an anti-alias filter to the seismic sampling rate of 4ms. The input reflectivity waveforms and impedance values were derived from synthetic seismograms rather than from the real data volumes. Synthetic seismic was preferred in the training phase because this ensured complete alignment between input and output traces over the entire target interval. With real seismic data we are always dealing with mis-picks and log-trace depth-to-time conversion problems resulting in unaligned data that degrades the training set. Synthetic seismograms and log traces are per definition aligned because they are converted from depth-to-time using the same sonic log. The trained network can thus find the optimal mapping between seismic input and target response. Application of such a 'perfect filter' does not remove any mis-picks and stretch / squeeze problems inherent to the seismic data. Before applying the trained network to real seismic data, the input must be scaled to the range of the synthetic response on which the network was trained.

Porosity prediction

Although porosity does not change over time, the seismic response does as a result of production. To avoid mapping production-induced changes to variations in porosity it was decided to predict porosity from all 10 available seismic cubes simultaneously, i.e. from both acquisition times (Fig. 2a). For reasons explained above the training set was constructed from logs and synthetic seismograms. Mid- and far-angle reflectivity synthetics in 1991 and 1997 were made from time-equivalent sonic and density logs by the convolutional method. Each synthetic had its own wavelet, which was an average over many wells. The time-

equivalent logs had been corrected for fluid changes with a modified version of the Gassmann equation. The saturation curves needed for the correction came from reservoir simulator predictions at times 1991 and 1997. Elastic impedance logs were derived from time-equivalent sonic, shear-sonic and density logs using Shuey's approximation:

$$Z_q = Z_p \exp([\log(Z_p) - 2\log(Z_S) + \log(5 \times 10^6)]\sin^2(\theta)),$$

where θ is the average angle of incidence in the target zone, and Z_q, Z_p, and Z_S, are the elastic impedance, acoustic impedance and shear impedance, respectively.

Two more inputs were fed to the neural network. The reference time relative to the Top Brent horizon was given to model vertical porosity trends in the reservoir. The second input was an indicator to reflect the distinctly different structural styles in the field. The main part of the field is a relatively undisturbed block of westerly dipping layers. The East flank is structurally complex and consists of tilted and rotated fault blocks with slumped deposits (Fig. 1). For each part, a different relation may exist between seismic and porosity. Rather than modelling separate networks for each area it was decided instead to supply the network with an environment indicator. The value zero indicated a location within the main area while a value of one was used for the East flank.

Out of the 130 available wells, some 30 were set aside to test the performance of the network. The remainder were used to create a training set. The entire Brent interval covers a time-window of approx. 150 ms. With a 4 ms-sampling rate this meant that the total number of training examples was approximately (100 × 150)/4 or 3750 vectors (the actual number was slightly less because intervals with missing logs are discarded). The network was quite able to find the desired relationship between seismic and porosity. The trained network was tested at blind test locations by applying it to both the synthetic responses and the (scaled) real seismic responses. Apart from an overall discrepancy in frequency content between actual – and neural network predicted porosity, the predictions at these blind test locations were deemed successful (Fig. 3). The low frequency of the predictions from real data reflected the band-limited frequency content of the seismic and inverted impedance cubes. The latter were made without broadening the frequency bandwidth.

Application of the trained network to the seismic data sets over a window of 150 ms hanging from the mapped top reservoir yielded the desired porosity volume (Fig. 3). The results corresponded well with the actual knowledge of the Brent Group. The Tarbert and Etive Formations clearly show the highest porosity, while Lower Ness, Rannoch and Broom Formations show up as lower porosity units.

Water saturation prediction

Variations in time-lapse signals were expected to be larger in porous rocks than in less porous rocks for two reasons. First, the effect of fluid replacement on the seismic response is more pronounced when porosity increases. Secondly, porosity is in general related to permeability. This implies that porous rocks are more easily drained than less porous rocks resulting in larger changes in saturation. The consequence of this reasoning is that porosity is a desired input for predicting saturation. This was also a feasible approach since porosity was now available at all sample positions in the target zone.

It may seem that we were hampering ourselves by including an input that was derived from the original seismic input without adding new information. This was not the case because additional information was in fact included in the process, albeit in a somewhat hidden manner. The network to predict porosity was focused on information from time-lapse (synthetic) seismic signals. The network to predict saturation concentrated on synthetic seismic responses as well, but now we were also utilizing information from porosity logs. Although we could have trained such a network at any time, there was no way of applying

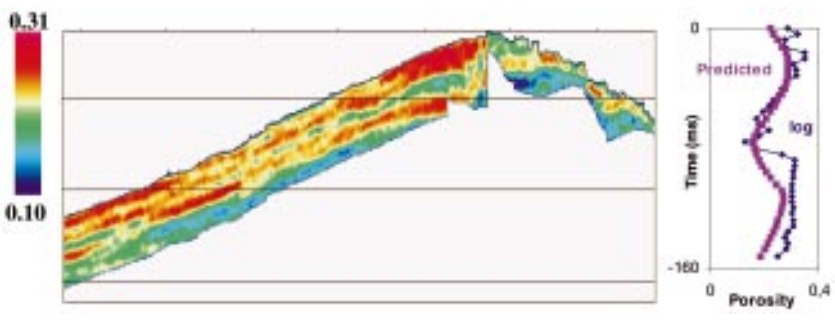

Figure 3 East–West profile through the porosity volume and a comparison between predicted and actual porosity at a blind test location.

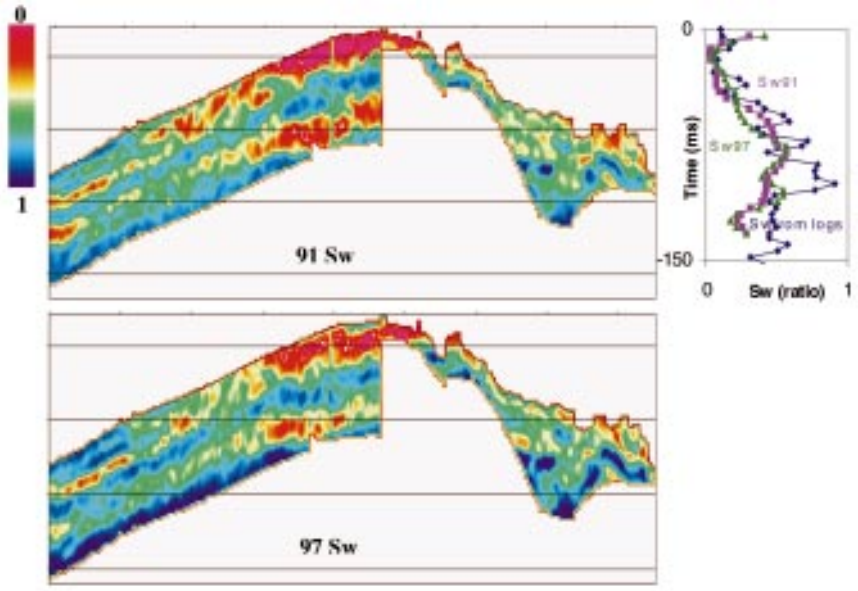

Figure 4 East–West profiles through 91 - and 97 saturation volumes and a comparison between predicted and actual saturation at a blind test well drilled in 91. Red indicates oil, blue is water.

it without predicting a porosity cube first.

We used one neural network to predict water saturation at different times. Applied to the 91 data set, the network predicted 91 water saturation, and applied to the 97 data set, it predicted 97 water saturation (Fig 2b). This can be explained as follows. Each well has a set of measured and derived logs (sonic, shear sonic, density, porosity, water saturation, mid- and far elastic impedance and acoustic impedance). Each set represents a consistent combination of inputs and target responses from which examples were extracted every 4ms over the entire target zone. By using all wells to train the neural network, we ensure that the set of measured logs does cover the entire range of possible variations. The elastic impedance logs were derived from the measured sonic, shear-sonic and density logs using the above mentioned Shuey's approximation. The shear sonic values required by this formula were predicted by a separate MLP neural network from measured gamma ray, sonic and density logs, for those wells lacking a shear sonic.

As with the porosity prediction, the network for predicting water saturation was trained on most of the 130 available wells. Five wells were used to test the network's performance as blind test locations. The neural network was applied to the same 150 ms interval hanging from the top reservoir. Application to the 91 data set yielded the desired 91 saturation volume and application to the 97 data resulted in the 97 saturation cube.

Results

Figure 4 shows the water saturation predictions at one of the blind test well locations. This particular well was drilled in 1991 and is located in the undisturbed main part of the field. For reasons explained above the frequency content of the predictions is lower than the frequency content of the actual water saturation trace. The predictions from the real seismic data matched the actual response quite well. Only slight time-lapse variations were observed. This would indicate that the saturation profile of this particular well has not changed much over a 7-year production period. Whether this corresponds with the observed production history remains to be studied.

Visual comparisons of 91 and 97 saturation predictions reveal the overall depletion in the main area of the field. Figure 4 shows an arbitrary inline through the respective saturation volumes. Red indicates low water saturation, hence oil, while blue indicates water. It shows that most oil is present in the porous upper and lower parts of the main area, i.e. in the Tarbert and Etive Formations. The East flank area only shows patches of oil, which makes sense given the disturbed sedimentation patterns. Detailed com-

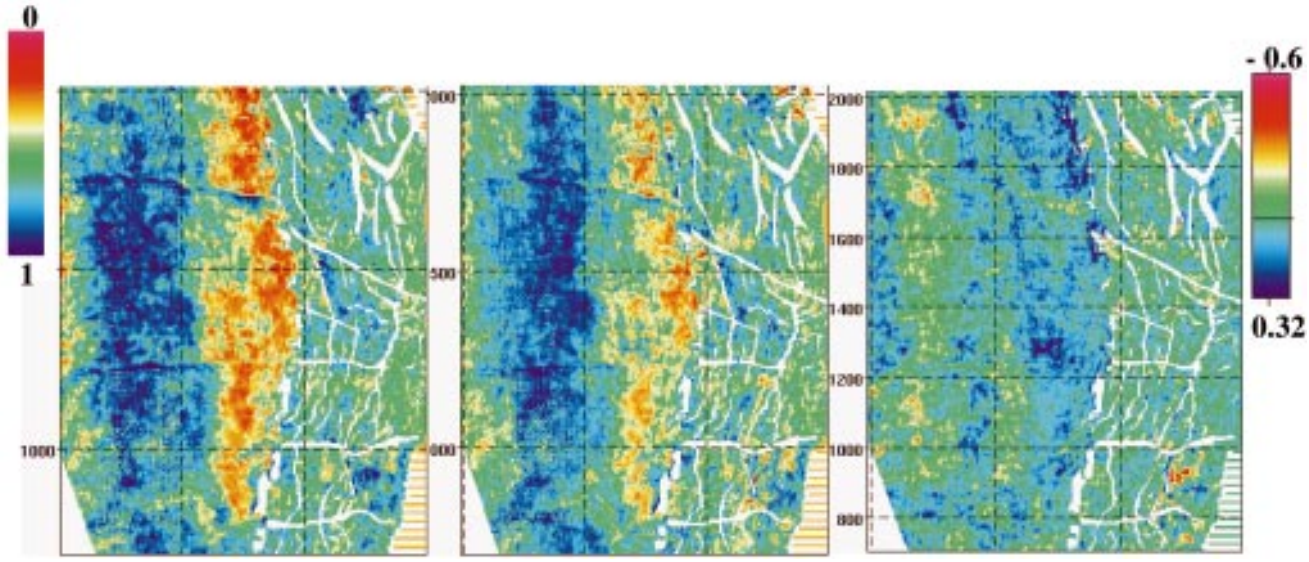

Figure 5 Slices at 12 ms below top reservoir through 91 - and 97 saturation volumes (left and middle, respectively). At right the difference (97 minus 91) is shown. Blue indicates flooding with water.

parison reveals that the oil saturation has decreased significantly in the Tarbert and Etive. Down flank oil patches present in the 91 data had been swept in 97.

Even more convincing is a comparison at stratigraphic level. Figure 5 shows the Southern part of the field. Slices were taken at 12 ms below the mapped top reservoir. In the main part of the field the 91 saturation is generally much higher than in 97. At the right the difference between the 91 and 97 water saturation is shown, where the former is subtracted from the latter. If the water saturation has increased, i.e. flooding with water occurred, then the difference is positive and indicated in blue. Red or green indicates respectively an increase in oil or no production at all. The difference plot reveals the overall level of depletion in the main area. North–South trends are visible, which may indicate permeability trends in the reservoir. The results for the East flank are more difficult to interpret. Some time-lapse differences were observed but in general the variations are small. This may either be a resolution / data quality problem in this difficult area, or it indicates that production has not yet had an impact on the seismic response.

Conclusions

A neural network was able to successfully predict from time-lapse seismic data the porosity and the 91 and 97 water saturation for the Brent Group in Statfjord. Porosity was predicted from all 10 available time-lapse data volumes simultaneously. The predicted porosity was subsequently used to predict water saturation at the respective seismic acquisition times. The results indicate an overall depletion of the main area. North–South drainage patterns were observed in a saturation difference slice through the porous upper Brent Tarbert Formation. The results for the East-Flank area are more difficult to interpret and require further study. All results remain to be validated against observed production behaviour and reservoir simulation predictions.

Acknowledgements

We like to thank Statoil and partners on Statfjord for using their data and permission to publish this paper.

References

Kirk, R.H. [1980] Statfjord field - A North Sea Giant, Giant Oil and Gas fields of the decade 1968-1978, AAPG memoir 30, edited by Halbouty, M.T.

Groot de, P.F.M. [1999] Volume transformation by way of neural network mapping, EAGE 1998, Helsinki.